Nuclear Engineering and Technology 55 (2023) 1031–1035

Contents lists available at ScienceDirect

Nuclear Engineering and Technology

journal homepage: www.elsevier.com/locate/net

Original Article

Monte-Carlo simulation for detecting neutron and gamma-ray simultaneously with CdZnTe half-covered by gadolinium film

J. Byun [a, b], J. Seo [a, b], Y. Kim [b, c], J. Park [a, d], K. Shin [a, d], W. Lee [d, e], K. Lee [e], K. Kim [e], B. Park [a, b, f, *]

[a] Dept. of Health and Safety Convergence Science, Korea University, Seoul, 02841, South Korea
[b] Interdisciplinary Program in Precision Public Health, Korea University, Seoul, 02841, South Korea
[c] Marine Radioactivity Monitoring Group, Korea Marine Environment Management Corporation, Busan, 48931, South Korea
[d] Transdisciplinary Major in Learning Health Systems, Graduate School, Korea University, Seoul, 02841, South Korea
[e] Dept. of Health and Environmental Science, Korea University, Seoul, 02841, South Korea
[f] Liquid Crystals Research Center, Konkuk University, Seoul, 05029, South Korea

ARTICLE INFO

Article history:
Received 17 September 2022
Received in revised form
12 October 2022
Accepted 3 November 2022
Available online 8 November 2022

Keywords:
Monte-Carlo simulation
Neutron detection
Prompt gamma-ray
Simultaneous detection
Gadolinium
CdZnTe

ABSTRACT

Neutron is an indirectly ionizing particle without charge, which is normally measured by detecting reaction products. Neutron detection system based on measuring gadolinium-converted gamma-rays is a good way to monitor the neutron because the representative prompt gamma-rays of gadolinium have low energies (79, 89, 182, and 199 keV). Low energy gamma-rays and their high attenuation coefficient on materials allow the simple design of a detector easier to manufacture. Thus, we designed a cadmium zinc telluride detector to investigate feasibility of simultaneous detection of gamma-rays and neutrons by using the Monte-Carlo simulation, which was divided into two parts; first was gamma-detection part and second was gamma- and neutron-simultaneous detection part. Consequently, we confirmed that simultaneous detection of gamma-rays and neutrons could be feasible and valid, although further research is needed for adoption on real detection.

1. Introduction

A neutron is an indirectly ionizing particle without a charge, which is normally measured by detecting reaction products. Detection systems of neutrons are determined depending on the neutron energy, where the thermal neutron is normally measured with reactions such as $^{10}B(n,\alpha)^{7}Li$, $^{6}Li(n,\alpha)^{3}H$, and $^{3}He(n,p)^{3}H$. However, in these cases, it is challenging to eliminate the gamma-ray signal acting as noise in (n, α) and (n, p) type detector, and to resolve the problem from wall effect that secondary charged ions (α and p) get lost by wall of detector [1]. Another way to detect the neutron is the measuring prompt gamma-rays [2], which are emitted after neutron capture of nuclei. For resolving the prompt gamma-rays, detectors with good energy resolution are needed.

CdTe-based semiconductor detectors [4–7] (i.e. CdTe, CdZnTeSe, CdMnTeSe etc) became commercialized and actively researched because of sufficient properties as gamma detectors such as high atomic number, prominent stopping power, wide band gap, transport property, and room-temperature operation. Mobility-lifetime product of electrons in CdZnTe(CZT) reached at 10^{-2} cm^2/V, and energy resolution on 662 keV gamma-ray energy were approximately from 1% to 3% when virtual Frisch grid (VFG) was introduced [8–10]. Thus, CZT with VFG could serve as a good energy resolution, which is needed for measuring the prompt gamma-rays.

There are three mechanisms to detect the neutron with CZT detector as shown in Fig 1. Fig. 1 (middle) shows a diagram of VFG CZT detector with converter, which converts neutrons to charged particles such as alpha and proton. However, a vacuum condition needs to be set to detect these charged particles, because converted particles can be shielded by ambient air while the prompt gamma-rays penetrate the air in ease. Given the geometry in Fig. 1 (right), the large volume of the detector is required because prompt gamma-rays taking place in a CZT detector should be attenuated in that detector [2]. Fig. 1 (left) shows the Gd-converted CZT detector,

* Corresponding author. Dept. of Health and Safety Convergence Science, Korea University, Seoul, 02841, South Korea.
E-mail address: pbj0116@korea.ac.kr (B. Park).

https://doi.org/10.1016/j.net.2022.11.002

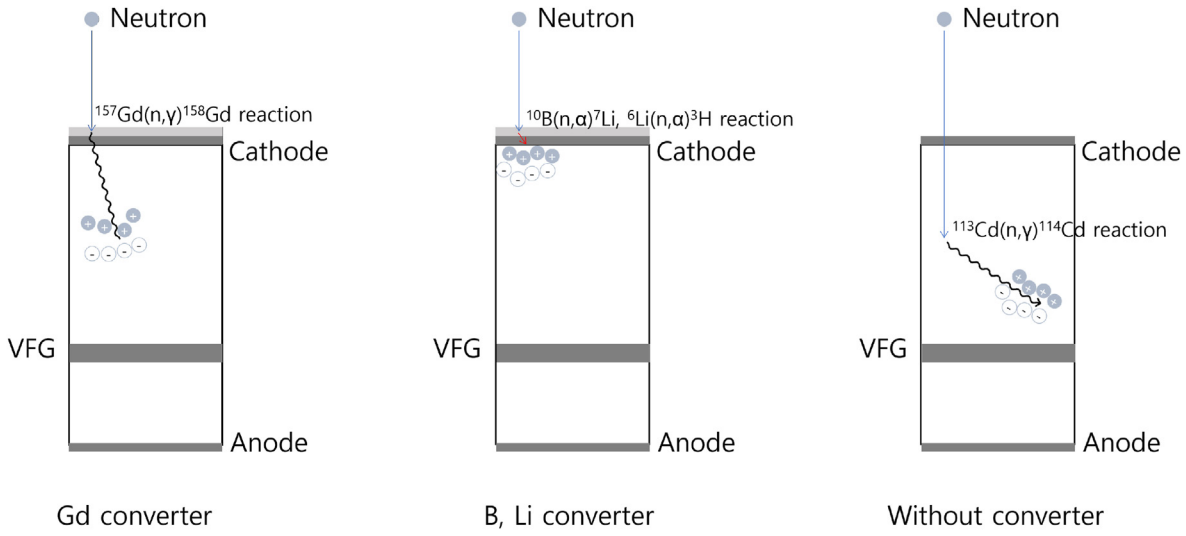

Fig. 1. Neutron detection mechanism using cadmium zinc telluride semiconductor detector. VFG means virtual Frisch grid.

which can be an ideal neutron detector. Moreover, gadolinium has a high cross-section on neutron [11], and energy of prompt gamma-ray emitted from Gd(n, γ) reactions is relatively lower than other prompt gamma-rays [3]. Low energy gamma-rays allow simple designs and thinness of the detectors, because low energy gamma-rays are easily absorbed with relatively thin materials. Thus, we choose the geometry in Fig. 1 (left) to design the neutron detector using the Monte-Carlo simulation. We divided a single CZT to two parts to investigate the feasibility of simultaneous detection of neutrons and gamma-rays with a single CZT detector; first was gamma-detection part and second was gamma- and neutron-simultaneous detection part.

2. Experiment

2.1. Neutron cross-section of gadolinium

Neutron cross-section of gadolinium was interpolated and reformed with IRDFF-1.0 data base [12]; where the interpolation and reformation were conducted using Matlab.

2.2. Monte-Carlo simulation

To carry out the Monte-Carlo simulation, MCNPX 2.5.0 version was used and ENDP/B-VI was selected as the nuclear data file. General geometry in MCNPX simulation was shown in Fig. 1 (left). To confirm an outbreak and relative intensity of prompt gamma-ray, MCNPX simulations with various thickness and isotopes of gadolinium converter were carried out, and the influence of neutron energy on intensity of prompt gamma rays was identified with two tally 4 or 8 function. After that, the optimized geometry was set to simultaneously measure the neutron and gamma-rays; the energy spectra of each pre-mentioned part of the CZT detector were simulated using tally 8 function. The energy spectrum of gamma-detection part was subtracted from the gamma- and neutron-simultaneous detection part.

3. Results and discussion

Natural isotopes of the gadolinium are ^{152}Gd, ^{154}Gd, ^{155}Gd, ^{156}Gd, ^{157}Gd, ^{158}Gd, and ^{160}Gd. Among them, high neutron cross-section results mainly from ^{155}Gd and ^{157}Gd, which have respectively

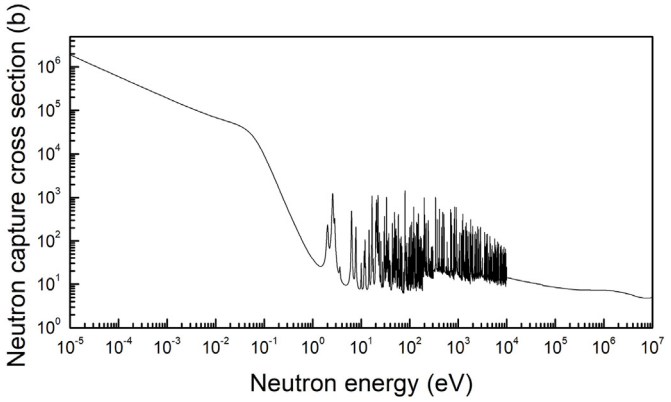

Fig 2. Neutron cross-section of gadolinium depending on energy of irradiated neutron [12].

60,900 and 254,000 (b, barn) in neutron cross-section [13]. Fig. 2 shows the neutron cross-section of gadolinium depending on the neutron energy. These values correspond to all Gd isotopes with amount of natural composition. Gadolinium absorbs well thermal neutrons that have a cross-section over 10^4 (b). After neutron absorption (neutron capture), prompt gamma-rays take place with energy in below equation (1 ~2) depending on the mass number of the reacted gadolinium.

$$^{155}Gd(n\ \gamma)^{156}Gd.\ \gamma - energy = 89\ and\ 199keV \quad (1)$$

$$^{157}Gd(n\ \gamma)^{158}Gd.\ \gamma - energy = 79\ and\ 182keV \quad (2)$$

To confirm the prompt gamma-rays emitted from ^{155}Gd and ^{157}Gd after neutron capture, energy spectra of the CZT detector were simulated with tally 8 function. Fig. 3 shows the prompt gamma-rays emitted after neutron capture of ^{155}Gd and ^{157}Gd. The thickness of gadolinium converter was set to 25 μm as mentioned in the prior study [13]. In Fig. 3 (left), prompt gamma-rays with 89 and 199 keV energies were measured, which result from $^{157}Gd(n\ \gamma)^{158}Gd$ reaction. In Fig. 3 (right), prompt gamma-rays with 79 and 182 keV energies were measured, which result from $^{155}Gd(n$

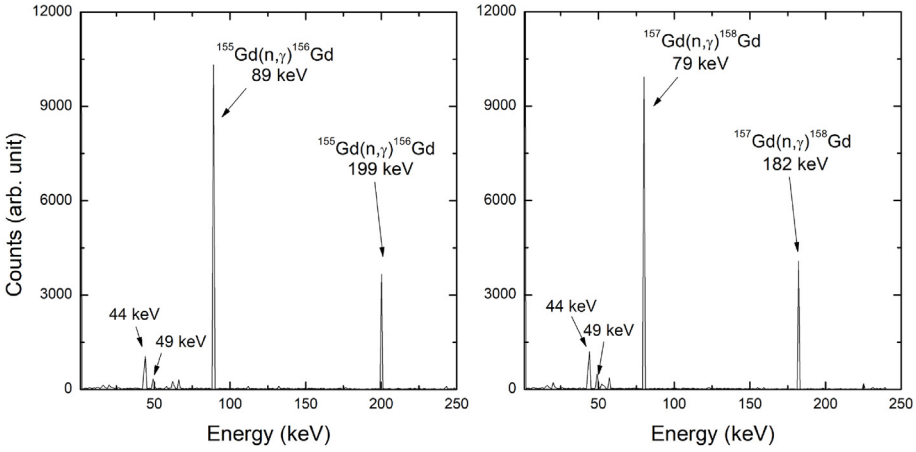

Fig. 3. Energy spectra of Gd-covered CZT detector simulated with MCNPX code. Where neutron energy was 0.25 eV and thickness of gadolinium was 25 μm.

$\gamma)^{156}Gd$ reaction. In both graphs of Fig. 3, the photon energy of 44 and 49 keV were measured, which are characteristic X-rays of gadolinium. The prompt gamma-rays from gadolinium were self-absorbed by the gadolinium converter, and the characteristic X-rays appeared, which were measured by the CZT detector. Thus, the mechanism doesn't depend on the converter if enough flux of prompt gamma-rays takes place, so both spectra in Fig. 3 show similar shape of characteristic X-rays of gadolinium.

Fig. 4 shows the energy spectrum of CZT with 25 μm gadolinium (Gd_{nat}) converter, which contains its isotopes with natural composition. All peaks shown in Fig. 3 are observed; however, other peaks are also observed in Fig. 4. The changed condition was only the Gd_{nat}, and it means that the peak energies except 43, 49, 79, 89, 182, and 199 keV were from the reaction with other gadolinium isotopes. (The detailed energies and their originated reaction are shown in Supplementary data.) However, others except

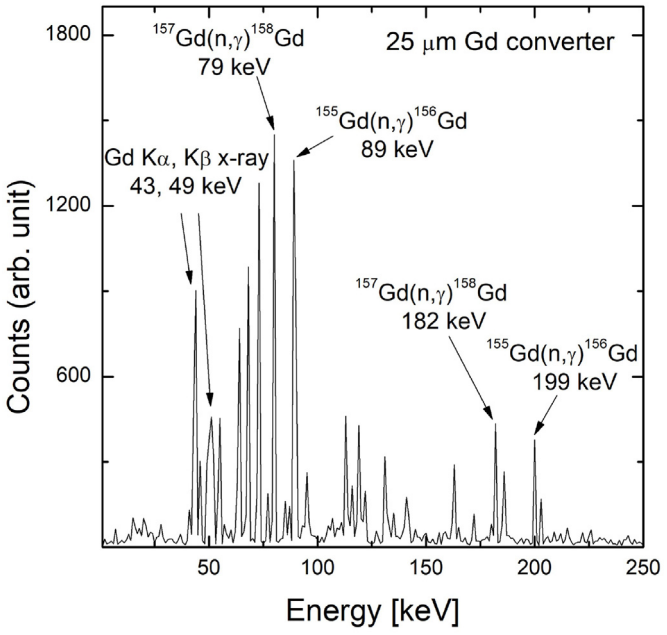

Fig. 4. Energy spectrum of Gd_{nat}-covered CZT detector simulated with MCNPX code. Neutron energy was set to 0.25 eV.

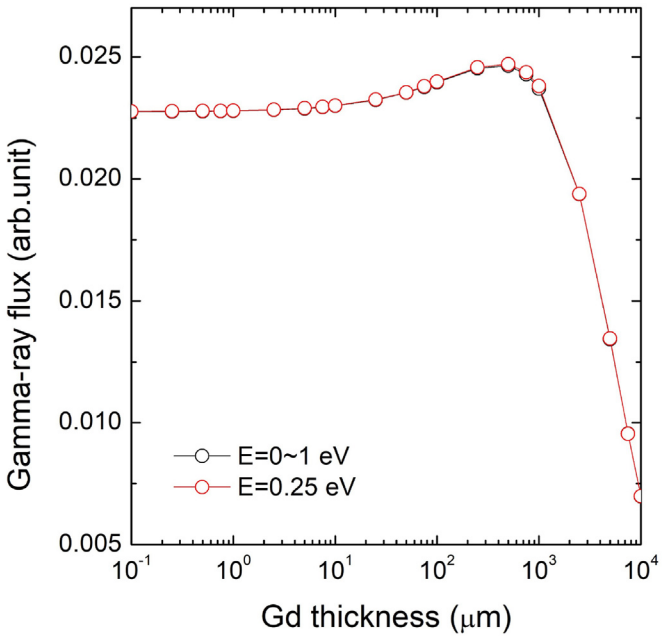

Fig. 5. Intensity of gamma-rays with increasing thickness of Gd_{nat}. Tally 4 was adopted to simulate intensity.

pre-mentioned peaks don't appear in real measurement with Gd-covered CdTe [3]. So, we judge that it was from a difference between the simulation and real measurement.

Fig. 5 shows intensities of gamma-rays with increasing thickness of gadolinium converter. Red symbols show the intensity when neutron energy is 0.25 eV, and the black symbols show the intensity when neutron energy is histogram setting (equally distributed from 0 to 1 eV). The 500 μm of Gd_nat has the highest intensity in both energies of neutrons. The increasing part is because of increasing thickness of Gd_{nat} which can react with neutrons and emit the prompt gamma-rays. However, when Gd_{nat} becomes thicker than certain thickness (500 μm), it can self-absorb the gamma-rays, which are caused by $Gd(n\ \gamma)$ reaction, thereby resulting in the decrease of gamma-ray intensity. The difference of intensity depending on the neutron energy was rare, if the energy is included the range in which the thermal neutron is classified.

To identify detailed information of intensity, we conducted tally 8 function with same geometry in Fig. 5. Fig. 6 shows the result of

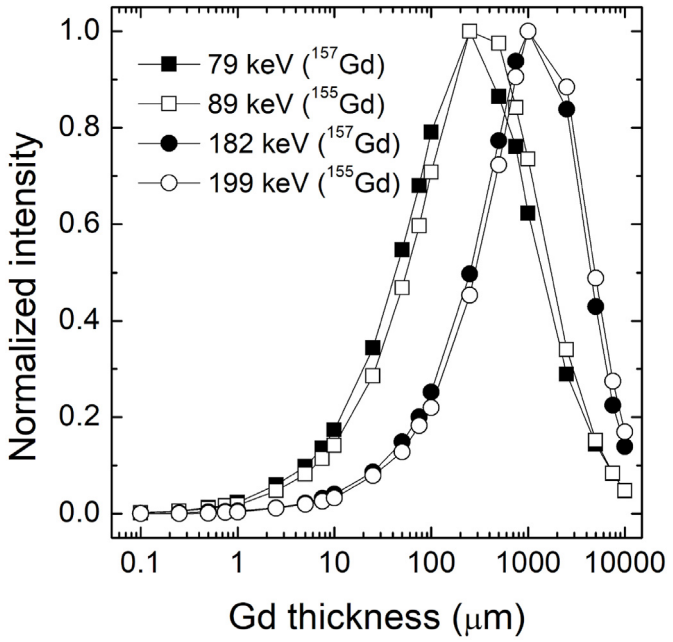

Fig. 6. Normalized intensity of prompt gamma-rays emitted from *Gd*(n γ) reaction. Where X axis is thickness of Gd_{nat} and Y axis is the normalized gamma-rays intensity.

the tally 8, where the neutron energy was set to 0.25 eV and the thickness of Gd_{nat} changed from 10^{-1}–10^{4} μm. The maximum intensities of 79 and 89 keV appear in 250 μm, and maximum intensities of 182 and 199 keV appear in 1000 μm. The reason why intensities of the former appear in thinner Gd_{nat} corresponds with the energy of prompt gamma-rays. Gamma-rays with higher energy have bigger penetration depth, so prompt gamma-rays are relatively free from the self-absorption. Thus, the maximum intensity of lower energy gamma-rays (79 and 89 keV) is located in the thinner thickness of Gd_{nat}.

After investigating the intensity of each prompt gamma-ray depending on thickness of Gd_{nat}, proper geometry for the simultaneous detection with CZT detector half-covered by Gd_{nat} was set as shown in Fig. 7. The thickness of Gd_{nat} converter was set to

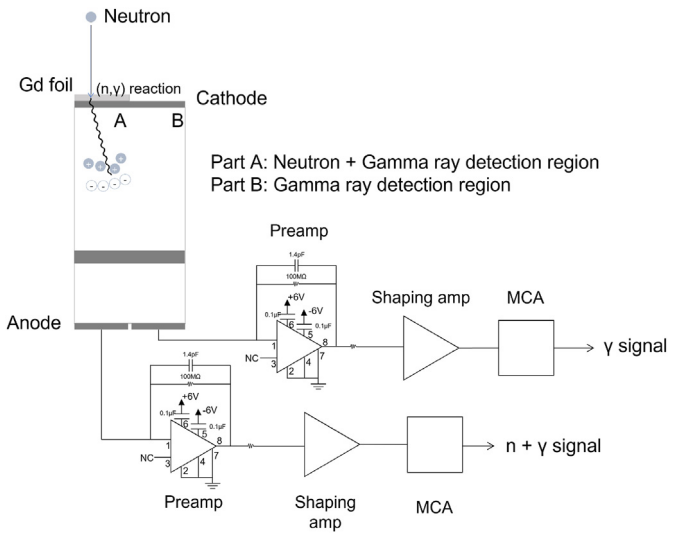

Fig. 7. Geometry of CZT half-covered by Gd_{nat} converter for detecting neutron and gamma-ray simultaneously.

250 μm, at which the maximum intensity of 79 and 89 keV energies in Fig. 6 appears. To distinguish the signals from parts A and B in Fig. 7, the anode electrode should be divided into two parts when conducting real measurement with the geometry. Then, the signals from part A consist of the gamma-ray and neutron signals (exactly expressed as prompt gamma-ray) because of Gd_{nat} converter, and the signals from part B consist of just gamma-rays. The gamma-ray signals of each part will be same, if totally same physical dimensions of part A and B, enough detection time, and uniform source distribution are guaranteed. In fact, there are many restrictions; however, they are the solvable problems with further research after this feasibility study. It should contain the research about angle-dependence,source position-dependence, neutron energy-dependence, and fabrication of a uniform geometry etc.

Fig. 8 displayed the spectra obtained with the geometry in Fig. 7. The CZT detector had a bar-type shape with physical dimension of $6 \times 6 \times 12$ mm^3. We added GEB function to simulation to identify that CZT and its energy resolution can be used for resolving prompt gamma-rays. So peaks in Fig. 8 were made broad like real detection with CZT detector unlike previous spectra (Figs. 3 and 4) that energy resolution was not set. As expected, the peaks of 662 keV gamma-rays emitted from ^{137}Cs were almost the same in both spectra obtained with part A and B. However, part B without Gd converter also detect prompt gamma-rays. If the prompt gamma-rays appearing in Gd converter penetrated depth of part A and absorbed in part B, the spectrum of part B can be explained because prompt gamma-rays are emitted to all directions. As an evidence of that, the prompt gamma-rays with relatively lower energies (79, 89 keV) in spectrum of part B have much lower intensity than that of prompt gamma-rays with higher energies (182, 199 keV), because of their relatively low penetration depth. With the same reason, characteristic X-rays appeared only in spectrum of part A. The blue line is the difference of both spectra. Its data contain only neutron information, meaning signals from 662 keV gamma-rays are fully subtracted. Thus, all peaks of prompt gamma-rays and

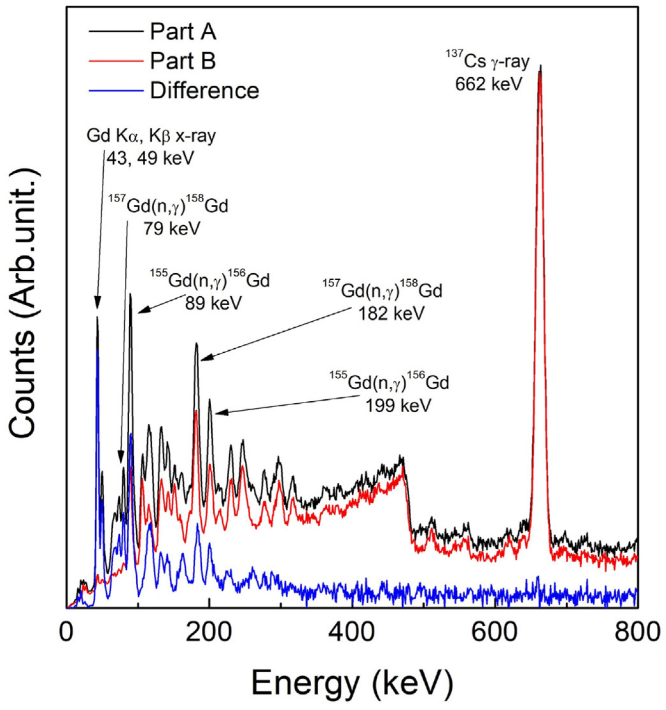

Fig. 8. Energy spectra of part A and B in CZT detector, and their difference. The part A was set to be covered by gadolinium film with thickness of 250 μm.

gamma-rays from isomeric transition of ^{137}Cs were observed and well-resolved in Fig. 8. These results can be a pilot study for application of the geometry on real detection in the radiation field mixed with neutrons and gamma-rays.

4. Summary

In this study, the feasibility of simultaneous detection of neutrons and gamma-rays was identified by using MCNP simulation. The prompt gamma-rays emitted from Gd(n γ) reaction were observed in the set geometry. Incident neutron energy rarely influenced to the intensity of the detected prompt gamma-rays, if the energy was included in the range of thermal neutron. Maximum intensity of prompt gamma-rays with energies of 79, 89, 182, and 199 keV appeared at 250, 250, 1000, and 1000 μm respectively. With selected setting and application of GEB function, the peaks of prompt gamma-rays after neutron capture and gamma-rays emitted by isomeric transition of ^{137}Cs were obtained together. Thus, it was confirmed that CZT detector half-covered by Gd converter can resolve prompt gamma-rays emitted from Gd(n γ) reaction and gamma-rays from isomeric transition. This result can be a good pilot study of application on detection at radiation field mixed with neutron and gamma-rays.

Declaration of competing interest

The authors declare that they have no known competing financial interests or personal relationships that could have appeared to influence the work reported in this paper.

Acknowledgments

This work was supported by the National Research Foundation of Korea (NRF) grant funded by the Korea government (MSIT) (No. 2020R1A2C2007376, 2021R1A2C1012161) and by Korea Institute of Energy Technology Evaluation and Planning (KETEP) grant funded by the Korea government (MOTIE) (20214000000070, Promoting of expert for energy industry advancement in the field of radiation technology).

Appendix A. Supplementary data

Supplementary data to this article can be found online at https://doi.org/10.1016/j.net.2022.11.002.

References

[1] G.F. Knoll, Radiation Detection and Measurement, John Wiley & Sons, 2010.
[2] D. McGregor, J. Kindsay, R. Olsen, Thermal neutron detection with cadmium$_{1-x}$ zinc$_x$ telluride semiconductor detectors, Nucl. Intrum. Meth. A. 381 (2-3) (1996) 498–501, https://doi.org/10.1016/S0168-9002(96)00580-3.
[3] A. Miyake, T. Nishioka, S. Singh, H. Morii, H. Mimura, T. Aoki, A CdTe detector with a Gd converter for thermal neutron detection, Nucl. Intrum. Meth. A. 654 (1) (2011) 390–393, https://doi.org/10.1016/j.nima.2011.06.083.
[4] H. Shiraki, M. Funaki, Y. Ando, A. Tachibana, S. Kominami, R. Ohno, THM growth and characterization of 100 mm diameter CdTe single crystals, IEEE Trans. Nucl. Sci. 56 (4) (2009) 1717–1723, https://doi.org/10.1109/TNS.2009.2016843.
[5] K. Kim, S. Cho, J. Suh, J. Hong, S. Kim, Gamma-ray response of semi-insulating CdMnTe crystals, IEEE Trans. Nucl. Sci. 56 (3) (2009) 858–862, https://doi.org/10.1109/TNS.2009.2015662.
[6] U.N. Roy, G.S. Camarda, Y. Cui, R. Gul, A. Hossain, G. Yang, J. Zazvorka, V. Dedic, J. Franc, R.B. James, Role of selenium addition to CdZnTe matrix for room-temperature radiation detector applications, Sci. Rep. 9.1 (2019) 1–7, https://doi.org/10.1038/s41598-018-38188-w.
[7] J. Byun, J. Seo, J. Seo, B. Park, Growth and characterization of detector-grade CdMnTeSe, Nucl. Eng. Technol. (2022), https://doi.org/10.1016/j.net.2022.06.007.
[8] K. Kim, S. Hwang, H. Yu, Y. Choi, Y. Yoon, A.E. Bolotnikof, R.B. James, Two-step annealing to remove Te secondary-phase defects in CdZnTe while preserving the high electrical resistivity, IEEE Trans. Nucl. Sci. 65 (8) (2018) 2333–2337, https://doi.org/10.1109/TNS.2018.2856805.
[9] Y. Kim, T. Lee, W. Lee, Radiation measurement and imaging using 3D position sensitive pixelated CZT detector, Nucl. Eng. Technol. 51 (5) (2019) 1417–1427, https://doi.org/10.1016/j.net.2019.03.009.
[10] Y. Kim, W. Lee, Development of a virtual Frisch-grid CZT detector based on the Array structure, J. Radiat. Prot. Res. 45 (1) (2020) 35–44, https://doi.org/10.14407/jrpr.2020.45.1.35.
[11] J. Dumazert, R. Coulon, Q. Lecomte, G.H.V. Bertrand, M. Hamel, Gadolinium for neutron detection in current nuclear instrumentation research: a review, Nucl. Intrum. Meth. A. 882 (2018) 53–68, https://doi.org/10.1016/j.nima.2017.11.032.
[12] E.M. Zsolnay, R. Capote Noy, H.J. Nolthenius, A. Trkov, Summary Description of the New International Reactor Dosimetry and Fusion File (IRDFF Release 1.0), International Atomic Energy Agency, No. INDC (NDS)–06162012, 2012.
[13] J. Dumazert, R. Coulon, V. Kondrasovs, K. Boudergui, Compensation scheme for online neutron detection using a Gd-covered CdZnTe sensor, Nucl. Intrum. Meth. A. 857 (2017) 7–15, https://doi.org/10.1016/j.nima.2017.03.018.